Journal of Applied Fluid Mechanics, Vol. 17, No. 3, pp. 548-558, 2024.
Available online at www.jafmonline.net, ISSN 1735-3572, EISSN 1735-3645.
https://doi.org/10.47176/jafm.17.3.2189

3D Numerical Modelling of Turbulent Flow in a Channel Partially Filled with Different Blockage Ratios of Metal Foam

A. Narkhede and N. Gnanasekaran†

Department of Mechanical Engineering, National Institute of Technology, Karnataka, Surathkal, Mangalore 575025, India

†Corresponding Author Email: gnanasekaran@nitk.edu.in

ABSTRACT

The aim of the present research work is to understand the intricacies of fluid flow through a rectangular channel that has been partially filled with a metal foam block of different blockage ratio (0.16-1), with a pore density (5–30 Pores Per Inch i.e. PPI), along with varying inlet velocity (6.5–12.5 m/s). For the porous region, numerical solutions are acquired using the Darcy Extended Forchheimer model. The Navier-Stokes equation is used in the non-porous zone. Different flow behaviours were seen as a function of PPI, height, and inlet velocity. The pressure drop increases with inlet velocity, PPI, and block height, with a maximum value of approximately 4.5 kPa for the case of 30 PPI, 12.5 m/s, and a blockage ratio of 1. Results show that the existence and location of the formation of eddies depends on the inlet velocity, PPI, and blockage ratio. Such studies have been reported less and will aid research on forced convection through a channel partially filled with metal foam and optimisation studies between increased heat transmission and the additional pressure drop for the same by providing a detailed fluid flow analysis.

Article History

Received July 30, 2023
Revised October 1, 2023
Accepted October 18, 2023
Available online January 1, 2024

Keywords:

Darcy Forchheimer
Metal foam
Pressure drop
Eddies
Partially filled channel
PPI

1. INTRODUCTION

Metal foam is extensively researched in recent years owing to its high surface-to-volume ratio, resulting in improved heat transfer. (Abdedou & Bouhadef, 2015; Anderson et al., 2015; Chand et al., 2015; Kamath et al., 2011; Mostafavi & Meghdadi Isfahani, 2017; Tikadar & Kumar, 2022; Li et al., 2023; Wang et al., 2023). Heat exchangers that make use of metal foam are receiving considerable attention (Boomsma et al., 2003; Ejlali et al., 2009; T'Joen et al., 2010; Odabaee & Hooman, 2011; Han et al., 2012; Muley et al., 2012, Odabaee & Hooman, 2012; Chumpia & Hooman, 2014; Nithyanandam & Singh, 2022). Numerous studies have demonstrated that open-cell metal foam improves the transfer of heat at the expense of pressure drop in the flow direction. (Anuar et al., 2017). So, rather than a completely packed arrangement, partially packed can be used to achieve reduction in pressure drop along with enhancement in transfer of heat over empty configurations (Kurtbas & Celik, 2009).

Hamadouche et al. (2016) performed experiments to study the drop in pressure and transfer of heat through a channel consisting of three aluminium foam blocks of 40 pore density and 93% porosity arranged in a staggered fashion on the lower and upper walls. Air velocity of 1-5 m/s with a constant thermal flux of 2 W/cm^2 at the lower wall was maintained. Results showed that the transfer of heat is approximately 300% for foam-packed channels in. Anuar et al. (2018a) conducted a study for the flow behaviour of air through a rectangular channel that has been partially packed with an aluminium foam block of PPI (5/10/30) with inflow velocity (3.9/5.5/6.2 m/s) and different blockage ratios using Particle image velocity and IR thermography techniques. The existence and location of recirculation zones vary for different values of PPI, height, and inlet velocity. Maximum drop in pressure was observed in tunnel 1 with a blockage value of 0.39, inflow velocity of 6.2 m/s, and a PPI of 30. This value was around 150 Pa/m. Sener et al. (2016) experimentally studied the drop in pressure and transfer of heat in a channel packed with aluminium foam. Reynolds number was maintained in the range of $968<Re_{Dh}<29624$ with air as a working fluid. For both laminar and turbulent flows, empirical equations are derived from experimental results. For a completely filled channel, the Thermal enhancement factor(TEF) is higher for 20 PPI than 10 PPI and for a partially packed case, TEF is always higher for 10 PPI. Lu et al. (2016) conducted an analytical investigation of the forced convection heat transmission and fluid flow behaviour in

NOMENCLATURE

C_F	Forchheimer coefficient	U	non-dimensionalized Streamwise velocity
d_f	fiber diameter	u_i'	fluctuation in mean velocity u_i
d_p	pore diameter	u_s	streamwise velocity
f	friction Factor	u_0	inlet velocity
H	height of channel	W	width of tunnel
h	height of metal foam	WT	wind Tunnel
$\frac{h}{H}$	blockage ratio	w	width of foam
K	permeability	Y	non-dimensional transversal coordinate
k	turbulent kinetic energy	ε	rate of energy dissipation
L	distance between the sections were pressures are measured for calculation of pressure drops	μ_{eff}	effective viscosity
L_T	tunnel length	μ_f	viscosity of fluid
l	foam length	μ_t	turbulent viscosity
PPI	Pores Per Inch	ρ_f	density of fluid
p	pressure	ν	kinematic viscosity
Δp	pressure drop across distance L	$\emptyset$	porosity

a parallel plate channel that was partially packed with metal foam of different porosities, PPI, and blockage ratio with constant thermal flux at the base. The transmission of heat and fluid motion depends on foam height. The temperature and velocity distributions were shown for the channel. Anuar et al. (2018b) conducted experiments to study the pressure and fluid motion for a rectangular channel that was partially packed with aluminium foam block for different inflow velocities, blockage ratio, and PPI using hot-wire anemometry and Laser Doppler Anemometry (LDA). Results were compared to those of the same size solid block. Kuznetsov (1996) analytically studied the fluid motion for different channels partially packed with porous media, considering the change in shear stress at the interface of clear fluid and porous media. Here, velocity profiles for different values of Darcy numbers were discussed with the implication of shear stress increment at the interface on them. Mancin et al. (2010) studied the fluid motion and heat transmission of air through Aluminium foam with 20 mm and 40 mm heights, constant porosity, 5-40 PPI, and 25, 32.5, and 40 kW/m^2 heat fluxes with variation in inlet velocity. The influence of velocity, height, and PPI on pressure reduction and global heat transfer was emphasized. The highest pressure loss was observed for the 40 PPI with 40 mm height and the least for 5 PPI foam with 20 mm height. Diani et al. (2014) considered a numerical study of airflow through high porosity metal foams having different PPI with almost the same porosity. It was reported that the pressure loss increases with inflow velocity and pore density. Xu et al. (2011) analytically investigated the fluid motion and heat transmission through a parallel plate channel that was partially packed with metal foam. Mass flow fraction in the metal foam region is highly driven by the hollow ratio, with a hollow ratio less than 0.3 giving superior performance compared to an empty channel.

Kouidri and Madani (2016) experimentally investigated the fluid flow behaviour of water through a heat exchanger packed with various foams (Copper, NiFeAlC, and Inconel). These samples are identical in terms of pore density (20 PPI) and pore size (1200 m), but they vary in ligament diameter and level of roughness. The pressure drops were analyzed for Copper(smooth), NiFeAlC(rough), and Inconel(highly rough) foams, pressure drops were more for the rougher one. Trilok et al. (2021) studied the fluid motion and heat transmission numerically through metal foam positioned in the center of a vertical channel. Here length, PPI, and porosity of foam are varied which resulted in different values of heat transmission and pressure losses. Moreover, the TOPSIS method was employed in order to balance pressure reduction and heat transfer. Shuja and Yilbas (2007) studied fluid motion and heat transfer numerically through a fixed width vertical channel with a rectangular porous block of different aspect ratios (4/2/1/0.5/0.25) and Porosity (0.899/0.972) with constant thermal flux for the block. Results were compared with a solid block. Nusselt number enhances and the Grashroff number reduces as the aspect ratio increased and the heat transmission rate from the block improves for higher porosities. Sung et al. (1995) conducted a numerical study of pressure losses and heat transmission for forced convection cooling in the printed circuit board with porous inserts. For different values of Da, Re, S, and R_k, the highest temperature recorded at the heat source and the resulting pressure losses are demonstrated. Bidar et al. (2016) performed a numerical investigation for fluid motion and heat transmission through a vertical channel packed with metal foams of various materials and compared the results to an empty vertical channel. The pressure drops were higher for higher velocities and lower values of porosity. Overall Nusselt number was higher for the packed channel, compared to the empty channel.

Jadhav et al. (2022) investigated heat transmission and flow of fluid through a circular conduit numerically, considering six different metal foam configurations. Aluminium foam of almost the same porosity (0.90-0.95) with PPI varying from 10 to 45 was considered and they were partially packed in the conduit to reduce the pressure drop while maintaining a constant thermal flux. The TOPSIS method was considered for balancing

pressure loss and thermal transmission. Liu et al. (2015) conducted an experimental parametric investigation for pressure drop and heat transfer coefficient for chilling supercritical carbon dioxide in tubes partially packed with foam, with different values of porosity (0.85/0.9/0.95) and PPI (20/40/60). As porosity increases, the heat transfer coefficient initially decreases, then increases, and the pressure drop decreases continuously. Heat transfer coefficient increases and pressure loss initially rise and then fall, with increase in pore density. Alkam and Al-Nimr (1999) performed a numerical investigation of the pressure loss and heat transmission in solar collector tubes that have porous substrates installed at the inner walls of the tubes. Nusselt number increased by 27 times with an increase of 15% to 130% in efficiency but there was an increase in pressure drop by 32 times. Dukhan et al. (2015) performed an experiment on an aluminium foam cylinder with constant thermal flux at the wall. It was shown that higher flow velocities resulted in a longer thermal entry length. It was more realistic to assume non-equilibrium thermal conditions at the local level.

From the above-mentioned literature, it is understood that more insights are required to understand the physics behind the fluid motion in configurations that are packed with metal foams in a partial manner. Most of the literature consists of forced convection through metal foam and optimisation studies related to increased heat transmission and the additional pressure drop in channels filled with metal foam. In the context of these studies, a comprehensive examination of fluid flow holds considerable importance, given its limited presence in the existing literature. Literature related to horizontal channels packed with metal foams in a partial manner is less reported. It is the role of the design engineer to consider the agreement between increased heat transmission and the additional pressure drop induced by metal foams in a partly foam-packed channel. This study examined numerically the behaviour of fluid flow through a rectangular channel packed with metal foams in a partial manner. The effect of inlet velocity, blockage ratio, and pore density on pressure drops and flow behaviour is shown.

2. PROBLEM STATEMENT AND METHODOLOGY

A wind tunnel (WT) with a horizontal orientation is considered, which is partially packed with metal foam (Anuar et al., 2018a). The foam is affixed to the WT's lower wall. The dimensions of WT are 1200 mm (L_T), 320 mm (W), 320 mm (H) and of metal foam are 270 mm (l), 320 mm (w), height (h). h is considered as 0.16, 0.25, 0.5, 0.75 & 1 times of H in this study. In the present investigation, the length of WT is 1200 mm, and the foam is 270 mm, so the entrance and exit effects on the flow are eliminated. Three different velocities 6.5, 9.5, and 12.5 m/s are taken at the inlet. The Reynolds numbers for this study is in the range of 135,000-265,000 for the velocity range of 6.5-12.5 m/s. For foam, 5, 10, and 30 PPI are considered.

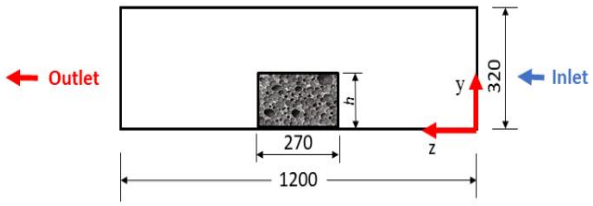

Fig. 1 Front view of computational domain

2.1 Computational Domain, Mesh and Boundary Conditions

To capture the pressure at the flow sections of WT, a three-dimensional domain is considered over a two-dimensional domain. The front view of the domain is shown in Fig. 1 for better understanding. To obtain a superior solution incorporating fewer cells, finite number of Hexahedral cells are used to discretize the domain. For the boundary conditions at the entrance and the outlet, velocity and the pressure of fluid are specified respectively. Different velocities 6.5-12.5 m/s at the entrance, and 1 atmospheric pressure at the outflow section are considered. Interior type condition is given at the clear fluid-metal foam interface i.e. shear stress is continuous at the interface, as suggested by many researchers (Kotresha & Gnanasekaran, 2020; Jadhav et al., 2021).

2.2 Numerical Approach

Commercially available ANSYS FLUENT software is used to do the three-dimensional numerical simulation with working fluid as Air. For the clear fluid and metal foam region the viscous-standard k-epsilon (2 equation), standard wall function model is used (Narasimmanaidu et al., 2021). The zones of clear fluid and metal foam, are both subjected to fluid flow. The assigned governing equations for the clear fluid region are the same as the empty channel flow. The metal foam region's governing equations include the terms of foam drag, permeability, and porosity. In the present study turbulent flow is considered inside the metal foam, based on the value of the permeability-based Reynolds number. The flow becomes turbulent when permeability-based Reynolds number is >100 (Nield & Bejan, 2005).we have consider the following set of governing equations for the metal foam zone: (Kotresha & Gnanasekaran, 2020; Jadhav et al., 2021)

Continuity Equation:

$$\frac{\partial\left(\rho_f \emptyset u_i\right)}{\partial x_i} = 0 \tag{1}$$

Momentum Equation:

$$\frac{\partial\left(\rho_f u_i u_j\right)}{\partial x_j} = -\emptyset\frac{\partial p}{\partial x_i} + \frac{\partial}{\partial x_j}\left(\left(\mu_f + \mu_t\right)\left(\frac{\partial u_i}{\partial x_j} + \frac{\partial u_j}{\partial x_i}\right)\right) - \emptyset\left(\frac{\mu_{eff}}{K}u_i + \frac{\rho_f C_F}{\sqrt{K}}uu_i\right) \tag{2}$$

Table 1 Properties of Metal foams (Anuar et al., 2018a)

Parameters	Values		
Pore density(PPI)	30	10	5
Porosity,$\emptyset(-)$	0.94	0.91	0.92
Permeability,$K * 10^{-7}(\mathrm{m}^2)$	0.37	1.65	2.61
Fiber diameter, d_f(m)	0.00027	0.00044	0.0011
Pore diameter, d_p(m)	0.00087	0.0026	0.0058

Table 2 Grid independence study

Number of elements	Inlet pressure (Pa)
204800	59.35
245760	58.98
307200	58.62
409600	58.66
614400	58.97

Table 3 Validation with experimental results

Inlet Velocity, $u_0\left(\frac{\mathrm{m}}{\mathrm{s}}\right)$	Pressure Gradient, $\frac{\Delta p}{L}\left(\frac{\mathrm{Pa}}{\mathrm{m}}\right)$	
	Present work	Experimental work (Anuar et al., 2018a)
6.5	51.5	47
9.5	108	100
12.5	186	180

Turbulent kinetic energy equation:

$$u_j \frac{\partial k}{\partial x_j} = -u_i{}' u_j{}' \frac{\partial u_i}{\partial x_j} + \frac{\partial}{\partial x_j}\left(\frac{K_m}{\sigma_k}\frac{\partial k}{\partial x_j}\right) - \varepsilon \tag{3}$$

Rate of energy dissipation equation:

$$u_j \frac{\partial \varepsilon}{\partial x_j} = -C_{\varepsilon 1}\frac{\varepsilon}{k} u_i{}' u_j{}' \frac{\partial u_i}{\partial x_j} + \frac{\partial}{\partial x_j}\left(\frac{K_m}{\sigma_\varepsilon}\frac{\partial \varepsilon}{\partial x_j}\right) - C_{\varepsilon 2}\frac{\varepsilon^2}{k} \tag{4}$$

Effective viscosity:

$$\mu_{eff} = \mu_f \tag{5}$$

Where,

$$\mu_t = \rho_f C_\mu \frac{k^2}{\varepsilon},\ K_m = \nu\left[1 + \left(\frac{C_\mu}{\nu}\right)\frac{k}{\varepsilon^{0.5}}\right]^2$$

Where,

$$C_\mu = 0.09; \sigma_k = 1.0; \sigma_\varepsilon = 1.3; C_{\varepsilon 1} = 1.44;\ C_{\varepsilon 2} = 1.92;$$

$$C_F = 0.00212 * (1-\emptyset)^{-0.132} * \left(\frac{d_f}{d_p}\right)^{-1.63} \tag{6}$$

For early convergence, the Green-Gauss Node based as gradient and the coupled scheme for pressure velocity coupling are considered. So, as compared to other schemes the computational time is reduced with the same accuracy in the final results. For the residuals i.e. continuity, and velocities, the convergence criteria are set as 10^{-4}. The properties of metal foam selected for numerical study are mentioned in Table 1.

2.3 Grid Independence Study

An integral aspect of any numerical solution is investigating grid independence. Here, the mesh is refined until the change in the results comes within the tolerance limit and further refining increases only the computational time without much change in results. Such a solution is called a grid-independent solution. In the present study, elements of 204800, 245760, 307200, 409600, and 614400 are considered. The inlet pressure does not change much for this range of the number of elements as shown in Table 2; so, 307200 elements have been considered to avoid higher computational time as required for the larger number of elements for the same accuracy in results.

3. RESULTS AND DISCUSSION

3.1 Validation with Experimental Results

To validate the method, a 5 PPI metal foam block of 0.16 blockage ratio with 6.5, 9.5, and 12.5 m/s inlet velocities are considered. The validation is shown in Table 3, the pressure gradient is considered and validated (Anuar et al., 2018a).

3.2 Velocity Profiles

Figure 2-4, illustrates the change of normalized stream-wise velocity, U along the non-dimensional transversal coordinate, Y with variation in PPI for $\frac{h}{H} = 0.5$ at inlet velocities of 6.5, 9.5, and 12.5 m/s, respectively. It can be observed that the values of U and velocity profiles are almost the same even though the inlet velocity is changing for a particular flow section, PPI, and blockage ratio.

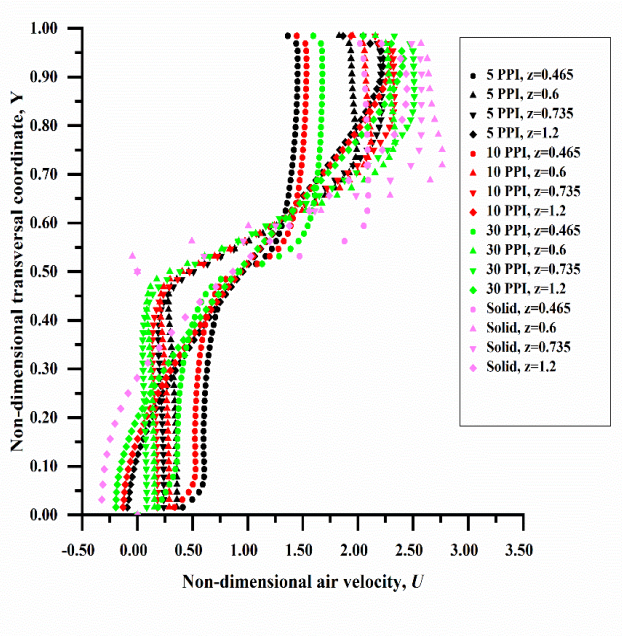

Fig. 2 Velocity Profiles for different PPI at different axial location for $\frac{h}{H} = 0.5$ and u_0=6.5 m/s

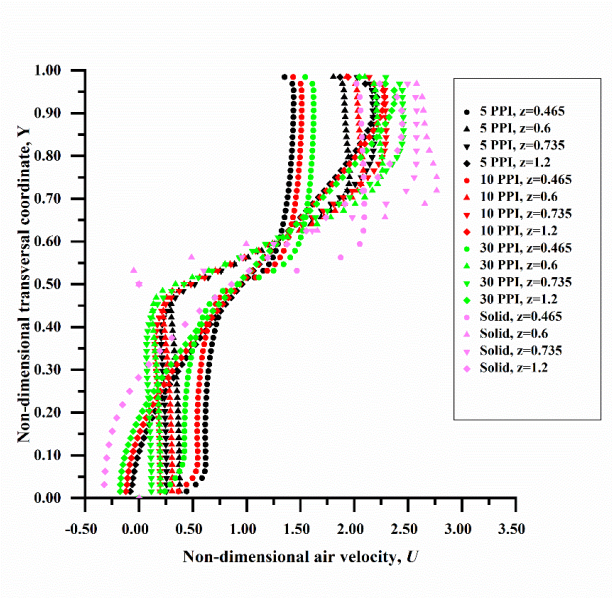

Fig. 3 Velocity Profiles for different PPI at different axial location for $\frac{h}{H} = 0.5$ and u_0=9.5 m/s

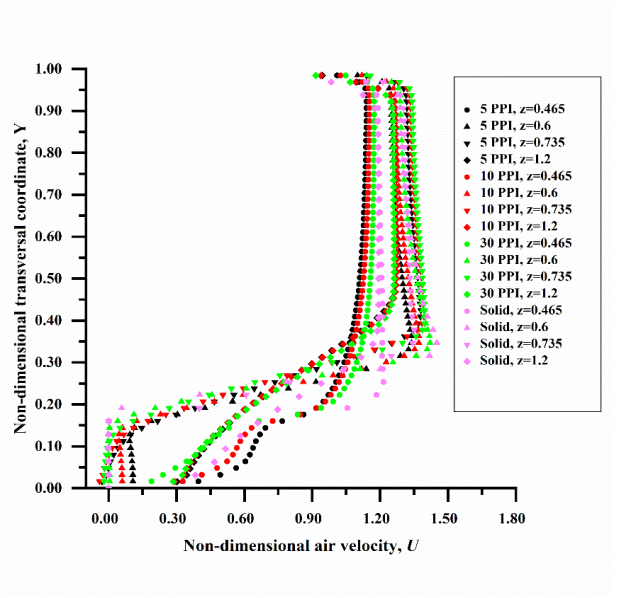

Fig. 5 Velocity Profiles for different PPI at different axial location for $\frac{h}{H} = 0.16$ and u_0 =6.5 m/s

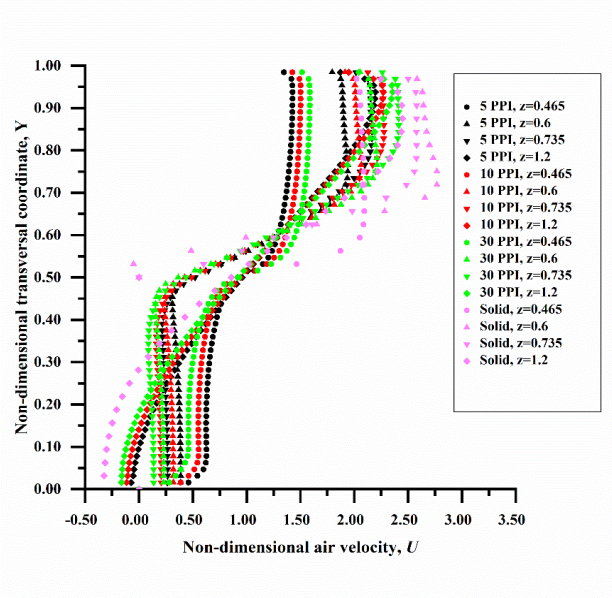

Fig. 4 Velocity Profiles for different PPI at different axial location for $\frac{h}{H} = 0.5$ and u_0=12.5 m/s

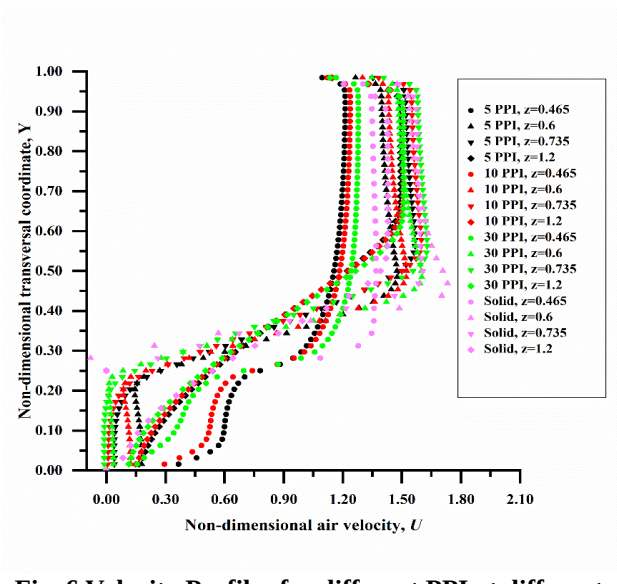

Fig. 6 Velocity Profiles for different PPI at different axial location for $\frac{h}{H} = 0.25$ and u_0=6.5 m/s

Figure 2 and Figs 5-7 show the variation of normalized stream-wise velocity U along the non-dimensional transversal coordinate, Y with variation in PPI at 6.5 m/s entrance velocity for blockage ratios of 0.5, 0.16, 0.25, and 0.75 respectively. At the section where the foam block starts (z=0.465 m), there is a sharp decrease in normalized stream-wise velocity U at the clear fluid-porous interface, regardless of the inlet velocity, blockage ratio, and PPI because due to resistance to the flow offered by the block, at z=0.465 more quantity of fluid will move to the clear fluid region above the metal foam block than the metal foam. This conclusion is consistent with the results shown in the experimental work (Anuar et al., 2018a).

For the flow section at the center of the foam (z=0.6 m), U in the clear fluid region above the metal foam especially the top of the channel is greater than the velocity at z=0.465 m for the same Y because, as fluid travels through the metal foam, some fluid continuously flows from the metal foam's upper surface into the clear fluid region. Due to the similar reason, for the flow section at the end of the foam (z=0.735 m), U in the clear fluid region above the metal foam especially the top of the channel is greater than the velocity at z=0.6 for the same Y. After the section z=0.735 m, the fluid in the clear fluid region above metal foam in the top portion of the channel expands due to which U at the exit of the channel (z=1.2 m) in the top portion of the channel is lower than the velocity at z=0.735 for the same Y.

Figure 2 and Figs 5-7 show that as the PPI increases, the normalized stream-wise velocity U increases in the top portion of the channel for any flow section, inlet velocity

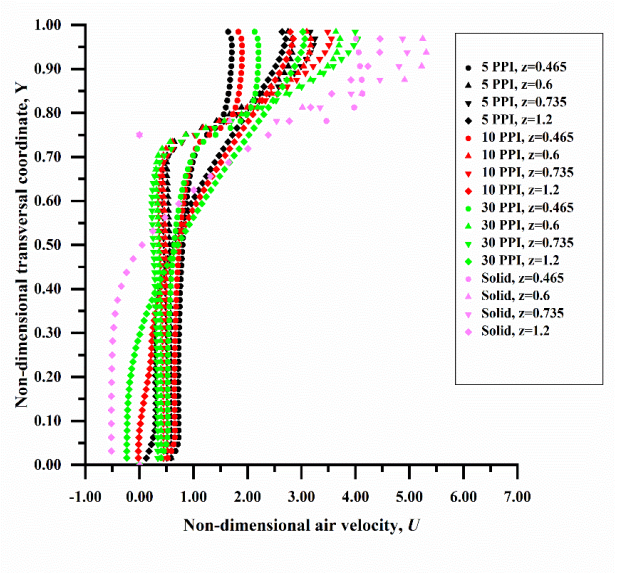

Fig. 7 Velocity Profiles for different PPI at different axial location for $\frac{h}{H} = 0.75$ and u_0=6.5 m/s

and blockage ratio because as the PPI increases the resistance to flow through metal foam increases and more quantity of fluid will try to flow from the clear fluid region above the metal foam.

Figure 2 and Figs 5-7 show that as the blockage ratio increases, the normalized stream-wise velocity U increases in the top portion of the channel for any flow section, inlet velocity, and PPI because resistance to flow by metal foam block increases.

3.3 Velocity Contours, Pressure Contours and Streamlines

Figure 8 shows the velocity contour, Pressure contour, and streamlines for $u_s = 12.5$ m/s and 30 PPI for different blockage ratios. So, for a particular PPI and inlet velocity as the blockage ratio increases, the flow through the metal foam block is less deviated from the z direction especially in the lower part of the block, as the fluid is trying to flow from the shortest possible path inside the metal foam to have the least resistance during flow. Due to this eddies formation shifts more and more towards the outlet.

Figure 9 shows the velocity contour, pressure contour, and streamlines for $u_s = 12.5$ m/s and $\frac{h}{H} = 0.5$ for different PPI. So, for a particular inlet velocity and blockage ratio as PPI increases more quantity of fluid tries to go from the top of the block without entering it as resistance to flow through the block increases, due to which the deviation of the fluid flowing through the metal foam from the z direction increases resulting in the formation of eddies closer to the metal foam block.

Figure 10 shows the velocity contour, pressure contour, and streamlines for 30 PPI and $\frac{h}{H} = 0.75$ for different inlet velocities. So, for a particular blockage ratio and PPI, the resistance offered by the block is the same, as inlet velocity decreases, fluid has more time to bend and flow from above the block without entering it. So, more quantity of fluid tries to flow above the block without entering it due to which the fluid flowing through the metal foam is more deviated from the z direction resulting in the formation of eddies closer to the metal foam block.

3.4 Pressure drop, friction factor and foam resistance coefficient

The pressure drop calculated between the two sections (z=0.395 m and z=0.805 m) mentioned in the present study is due to four reasons (1) Friction to flow due to channel walls. (2) Acceleration of fluid due to an

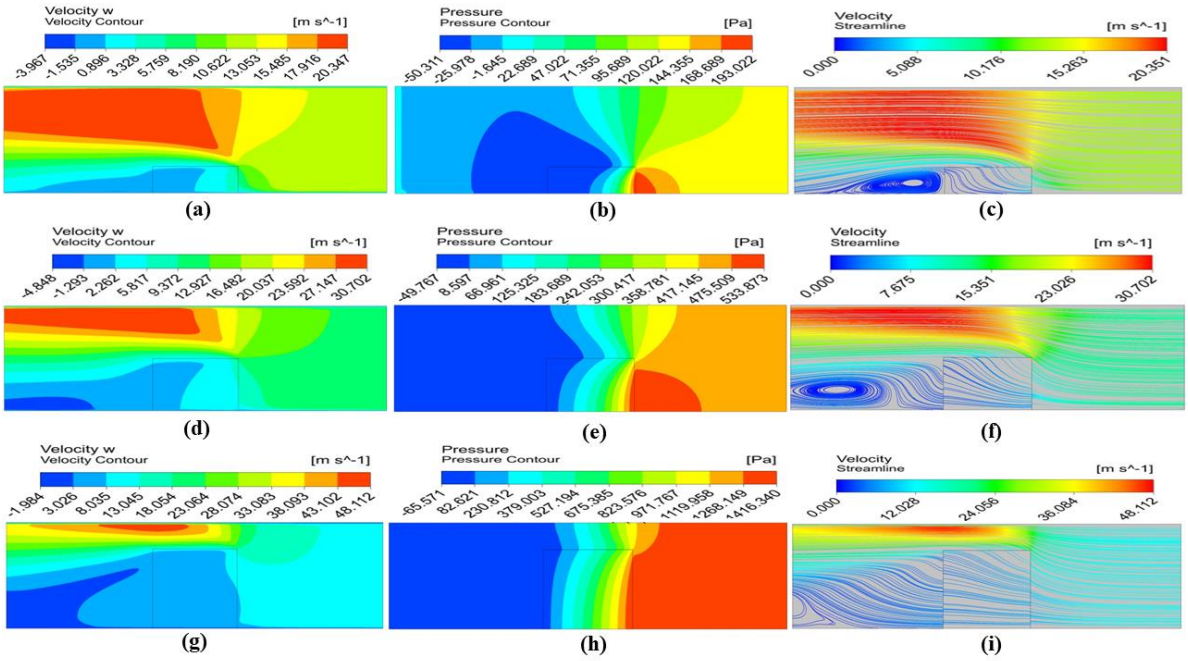

Fig. 8 Velocity contour, Pressure contour and streamlines for u_0=12.5 m/s and 30 PPI (a), (b) and(c) $\frac{h}{H} = 0.25$ (d), (e) and (f) $\frac{h}{H} = 0.5$ (g), (h) and(i) $\frac{h}{H} = 0.75$

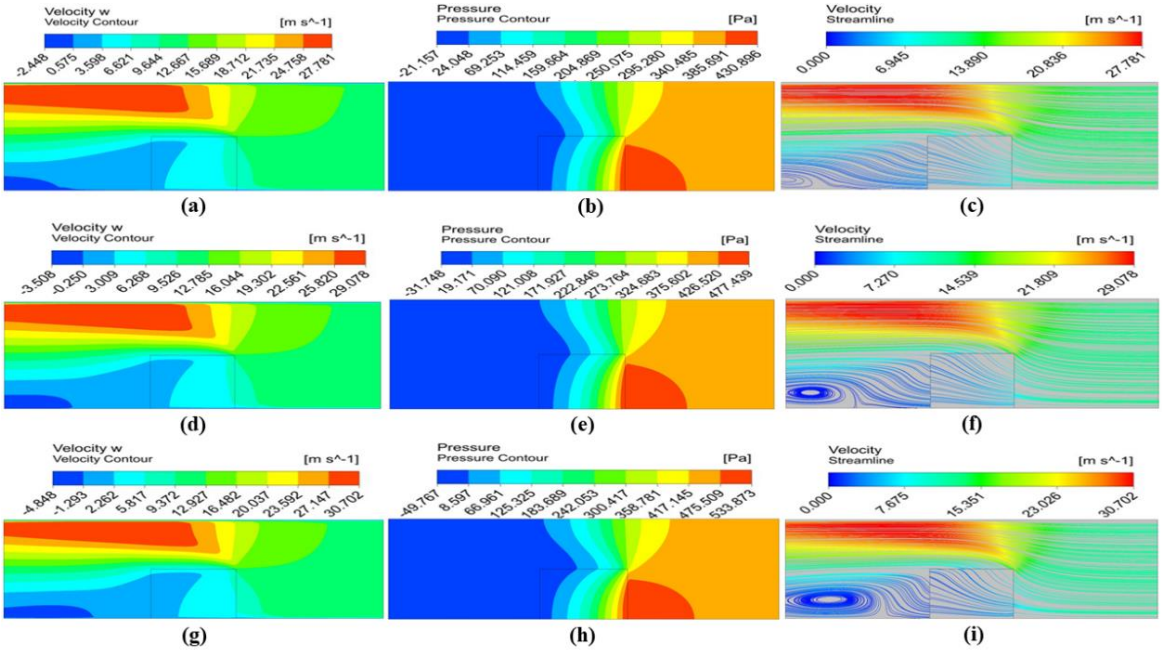

Fig. 9 Velocity contour, Pressure contour and streamlines for $u_0 = 12.5\ m/s$ and $\frac{h}{H} = 0.5$ (a), (b) and(c) 5PPI (d), (e) and (f) 10PPI (g), (h) and (i) 30PPI

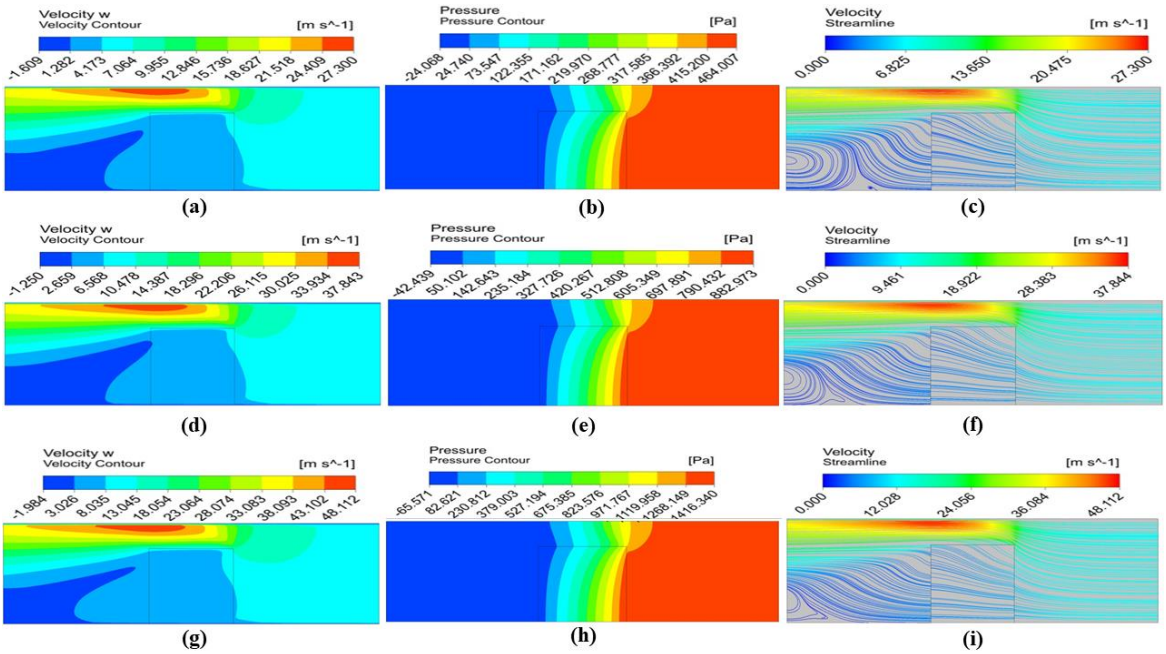

Fig. 10 Velocity contour, Pressure contour and streamlines for 30 PPI and $\frac{h}{H} = 0.75$ (a), (b) and(c) $u_0 = 6.5\ m/s$ (d), (e) and (f) $u_0 = 9.5\ m/s$ (g), (h) and (i) $u_0 = 12.5\ m/s$

decrease in flow area at the section where the porous block starts (z=0.465 m). (3) De-acceleration of fluid due to an increase in flow area at the section where the porous block ends (z=0.735 m). (4) Losses at the metal foam's top surface and Form drag, Skin-friction drag caused by ligaments.

So, formulation for pressure drop is shown in the following equations (Anuar et al., 2018a):

$$\Delta p = \Delta p_{channel} + \Delta p_{contraction} + \Delta p_{expansion} + \Delta p_{foam} \tag{7}$$

$$= k_{channel} * \frac{\rho_f {u_0}^2}{2} + k_{contraction} * \frac{\rho_f {u_0}^2}{2} + k_{expansion} * \frac{\rho_f {u_0}^2}{2} + k_{foam} * \frac{\rho_f {u_0}^2}{2} \tag{8}$$

Where,

$$k_{channel} = f_1 \frac{L}{D_h} \tag{9}$$

$k_{channel}$ is the channel resistance coefficient and f_1 is the friction factor for an empty channel that can be determined by use of the Darcy-Weisbach formula. Here even though a portion of channel's lower wall is removed by the base of the block, its effect on the total pressure drop will be negligible.

In a partially packed channel, the resistance to flow due to sudden contraction and sudden expansion is significant unlike in the case of a completely packed channel by foam where these resistances become negligible in front of the foam resistance. The formulas for the resistance coefficient of sudden contraction and expansion are shown in Eqs. (10) and (11):

$$k_{contraction} = \frac{1}{2} * \left[1 - \left(\frac{H-h}{H}\right)^2\right]^2 \tag{10}$$

$$k_{expansion} = \left(1 - \frac{(H-h)}{H}\right)^2 \tag{11}$$

k_{foam} is the foam resistance coefficient, it accounts for the foam drag, shear drag, and viscous drag of metal foam, as well as minor loses above the foam in the clear flow region. So, from Eqs. (8), (9), (10) and (11) we can write the following equation:

$$k_{foam} = \frac{2\Delta p}{\rho_f {u_0}^2} - f_1 \frac{L}{D_h} - \frac{1}{2} * \left[1 - \left(\frac{H-h}{H}\right)^2\right]^2 - \left(1 - \frac{(H-h)}{H}\right)^2 \tag{12}$$

The formulation for friction factor of the channel packed with metal foams in a partial manner is shown in equation (Anuar et al., 2018a):

$$f = \frac{2\Delta p D_h}{\rho_f {u_0}^2 L} \tag{13}$$

Figure 11 and Fig. 12 show the pressure gradient variation with blockage ratio for various entrance velocities and pore densities. The pressure gradient increases with inlet velocity for a particular blockage ratio and PPI, as the resistance to flow due to metal foam, channel walls, sudden contraction, and sudden expansion increases. For a given inlet velocity and PPI, the pressure gradient rises as the blockage ratio increases, as the resistance to flow due to metal foam, sudden contraction, and sudden expansion increases. For the spectrum of blockage ratios addressed in the present work, the pressure gradient grows with increasing PPI for a given inlet velocity and blockage ratio, as the resistance due to metal foam increases. In some literature (Anuar et al., 2018a), for a lower blockage ratio the pressure gradient reduces with PPI for a particular inlet velocity.

Figure 13 illustrates the change in friction factor with blockage ratio for different inlet velocities and pore densities of metal foam, where f is calculated from Eq. (13). f reduces with entrance velocity for a particular blockage ratio and PPI, for the cases considered in Fig. 13. For a certain inlet velocity and PPI, f increases with blockage ratio. For a given inlet velocity and blockage

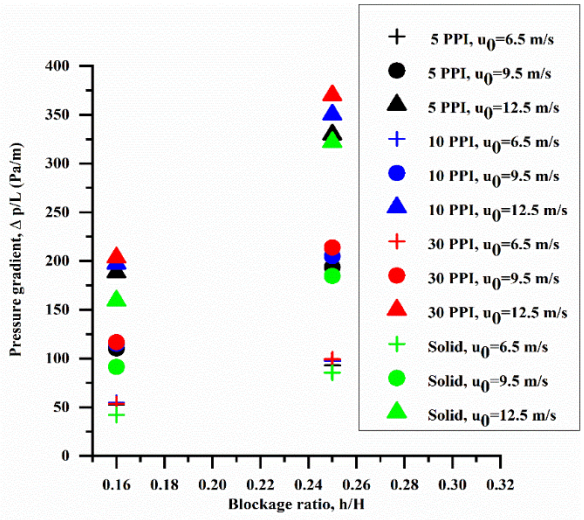

Fig. 11 Pressure gradient variation with blockage ratio for $\frac{h}{H} = 0.16$ and $\frac{h}{H} = 0.25$

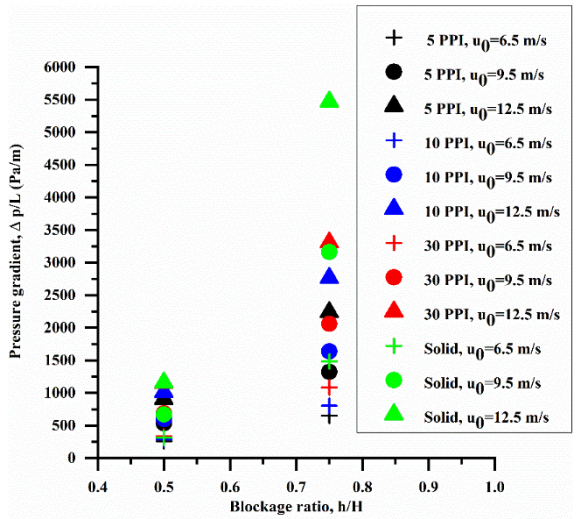

Fig. 12 Pressure gradient variation with blockage ratio for $\frac{h}{H} = 0.5$ and $\frac{h}{H} = 0.75$

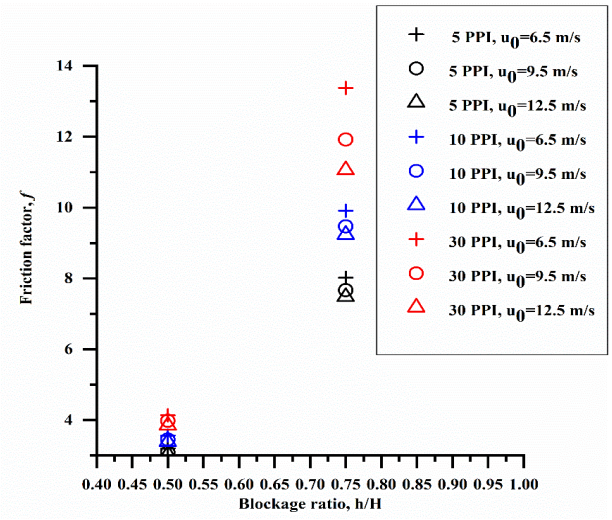

Fig. 13 Friction factor variation with blockage ratio for $\frac{h}{H} = 0.5$ and $\frac{h}{H} = 0.75$

ratio, f increases with PPI for the range of blockage ratios addressed here.

Figure 14 shows the variation of $k_{foam} * \frac{D_h}{L_f}$ with blockage ratio for metal foam with varying inlet velocities and pore densities, where k_{foam} is calculated from Eq. (12). k_{foam} reduces with inlet velocity for a particular blockage ratio and PPI, for the cases considered. For a given velocity and PPI, k_{foam} increases with the blockage. For a given velocity and blockage ratio, the coefficient k_{foam}, increases with PPI in the range of blockage ratios studied here.

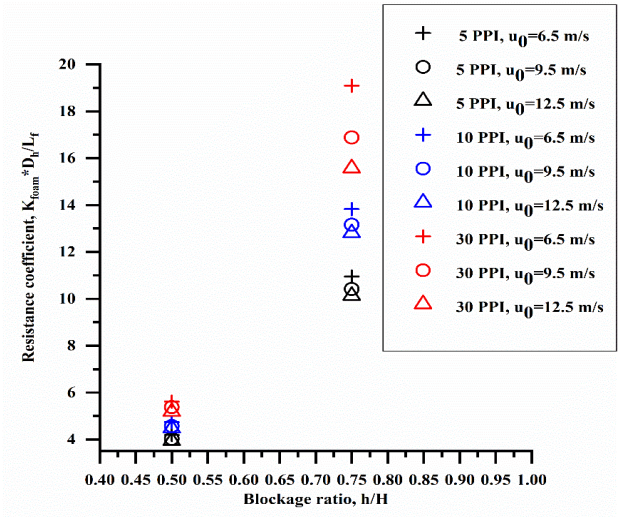

Fig. 14 Resistance coefficient variation with blockage ratio for $\frac{h}{H} = 0.5$ and $\frac{h}{H} = 0.75$

4. CONCLUSION

Numerical modelling of the behaviour of fluid flow through a rectangular channel packed with metal foams in a partial manner has been proposed. Variations in velocity profile, pressure drop, friction factor, resistance coefficient, and existence and location of formation of eddies for different inlet velocities, PPI, and blockage ratio were shown. The study concludes with the following findings.

- Velocity profiles for normalized stream-wise velocity are almost similar for different inlet velocities but vary with PPI and blockage ratio.
- The existence and location of the formation of eddies depend on PPI, inlet velocity, and blockage ratio. For higher PPI, lower inlet velocity, and lower blockage ratio, the eddies are formed closer to the metal foam block downstream of the foam.
- An increase in pressure drop occurs with PPI, blockage ratio, and inlet velocity with a maximum value of approximately 4.5 KPa for the case of 30 PPI, 12.5 m/s inlet velocity, and *h/H*=1.
- For cases studied here, the friction factor and Resistance coefficient both rise with PPI and the blockage ratio but fall with inlet velocity.

CONFLICT OF INTEREST

The authors declare that they have no known competing financial interests or personal relationships that could have appeared to influence the work reported in this paper.

AUTHOR CONTRIBUTION

A. Narkhede: Investigation, Software, Validation, Conceptualization, Methodology, Writing original draft, Visualization. **N Gnanasekaran**: Investigation, Visualization, Supervision, Writing, Review & editing.

REFERENCES

Abdedou, A., & Bouhadef, K. (2015). Comparison between two local thermal non equilibrium criteria in forced convection through a porous channel. *Journal of Applied Fluid Mechanics*, *8*(3), 491–498. https://doi.org/10.18869/acadpub.jafm.67.222.22233

Alkam, M. K., & Al-Nimr, M. A. (1999). Solar collectors with tubes partially filled with porous substrates. ASME. *Journal of Solar Energy Engineering*, *121*(1), 20–24. https://doi.org/10.1115/1.2888137

Anderson, K., Shafahi, M., & Gutierrez, A. (2015). Numerical study of forced air cooling of a heated porous foam pyramid array. *Journal of Applied Fluid Mechanics*, *8*(4), 727–734. https://doi.org/10.18869/acadpub.jafm.67.223.22675

Anuar, F. S., Abdi, I. A., Hooman, K. (2018a). Flow visualization study of partially filled channel with aluminium foam block. *International Journal of Heat and Mass Transfer*, 127, 1197–1211. https://doi.org/10.1016/J.IJHEATMASSTRANSFER.2018.07.047

Anuar, F. S., Abdi, I. A., Odabaee, M., Hooman, K. (2018b). Experimental study of fluid flow behaviour and pressure drop in channels partially filled with metal foams. *Experimental Thermal and Fluid Science*, 99, 117–128. https://doi.org/10.1016/j.expthermflusci.2018.07.032

Anuar, F. S., Malayeri, M. R., & Hooman, K. (2017). Particulate fouling and challenges of metal foam heat exchangers. *Heat Transfer Engineering*, *38*(7–8), 730–742. https://doi.org/10.1080/01457632.2016.1206415

Bidar, B., Shahraki, F., & Mohebbi-Kalhori, D. (2016). 3D numerical modelling of convective heat transfer through two-sided vertical channel symmetrically filled with metal foams. *Periodica Polytechnica Mechanical Engineering*, *60*(4), 193–202. https://doi.org/10.3311/PPme.8511

Boomsma, K., Poulikakos, D., & Zwick, F. (2003). Metal foams as compact high performance heat exchangers.

Mechanics of Materials, *35*(12), 1161–1176. https://doi.org/10.1016/j.mechmat.2003.02.001

Chand, R., Rana, G. C., & Hussein, A. K. (2015). On the onsetof thermal instability in a low prandtl number nanofluid layer in a porous medium. *Journal of Applied Fluid Mechanics*, *8*(2), 265–272. https://doi.org/10.18869/acadpub.jafm.67.221.22830

Chumpia, A., & Hooman, K. (2014). Performance evaluation of single tubular aluminium foam heat exchangers. *Applied Thermal Engineering*, *66*(1–2), 266–273. https://doi.org/10.1016/j.applthermaleng.2014.01.071

Diani, A., Bodla, K. K., Rossetto, L., & Garimella, S. V. (2014). Numerical analysis of air flow through metal foams. *Energy Procedia*, *45*, 645–652. https://doi.org/10.1016/j.egypro.2014.01.069

Dukhan, N., Baıci, Ö., & Özdemir, M. (2015). Thermal development in open-cell metal foam: An experiment with constant wall heat flux. *International Journal of Heat and Mass Transfer*, *85*, 852–859. https://doi.org/10.1016/j.ijheatmasstransfer.2015.02.047

Ejlali, A., Ejlali, A., Hooman, K., & Gurgenci, H. (2009). Application of high porosity metal foams as air-cooled heat exchangers to high heat load removal systems. *International Communications in Heat and Mass Transfer*, *36*(7), 674–679. https://doi.org/10.1016/j.icheatmasstransfer.2009.03.001

Hamadouche, A., Nebbali, R., Benahmed, H., Kouidri, A., & Bousri, A. (2016). Experimental investigation of convective heat transfer in an open-cell aluminum foams. *Experimental Thermal and Fluid Science*, *71*, 86–94. https://doi.org/10.1016/j.expthermflusci.2015.10.009

Han, X. H., Wang, Q., Park, Y. G., T'Joen, C., Sommers, A., & Jacobi, A. (2012). A review of metal foam and metal matrix composites for heat exchangers and heat sinks. In *Heat Transfer Engineering*, 33(12), 991–1009. https://doi.org/10.1080/01457632.2012.659613

Jadhav, P. H., G, T., Gnanasekaran, N., & Mobedi, M. (2022). Performance score based multi-objective optimization for thermal design of partially filled high porosity metal foam pipes under forced convection. *International Journal of Heat and Mass Transfer*, *182*. https://doi.org/10.1016/j.ijheatmasstransfer.2021.121911

Jadhav, P. H., Nagarajan, G., & Perumal, D. A. (2021). Conjugate heat transfer study comprising the effect of thermal conductivity and irreversibility in a pipe filled with metallic foams. *Heat and Mass Transfer/Waerme- Und Stoffuebertragung*, *57*(6), 911–930. https://doi.org/10.1007/s00231-020-03000-x

Kamath, P. M., Balaji, C., & Venkateshan, S. P. (2011). Experimental investigation of flow assisted mixed convection in high porosity foams in vertical channels. *International Journal of Heat and Mass Transfer*, *54*(25–26), 5231–5241. https://doi.org/10.1016/j.ijheatmasstransfer.2011.08.020

Kotresha, B., & Gnanasekaran, N. (2020). Numerical simulations of fluid flow and heat transfer through aluminum and copper metal foam heat exchanger–a comparative study. *Heat Transfer Engineering*, *41*(6–7), 637–649. https://doi.org/10.1080/01457632.2018.1546969

Kouidri, A., & Madani, B. (2016). Experimental hydrodynamic study of flow through metallic foams: Flow regime transitions and surface roughness influence. *Mechanics of Materials*, *99*, 79–87. https://doi.org/10.1016/j.mechmat.2016.05.007

Kurtbas, I., & Celik, N. (2009). Experimental investigation of forced and mixed convection heat transfer in a foam-filled horizontal rectangular channel. *International Journal of Heat and Mass Transfer*, *52*(5–6), 1313–1325. https://doi.org/10.1016/j.ijheatmasstransfer.2008.07.050

Kuznetsov, A. V. (1996). Analytical investigation of the fluid flow in the interface region between a porous medium and a clear fluid in channels partially filled with a porous medium. *Applied Scientific Research*, *56*.

Li, W. Q., Li, Y. X., Yang, T. H., Zhang, T. Y., & Qin, F. (2023). Experimental investigation on passive cooling, thermal storage and thermoelectric harvest with heat pipe-assisted PCM-embedded metal foam. *International Journal of Heat and Mass Transfer*, *201*, 123651. https://doi.org/10.1016/j.ijheatmasstransfer.2022.123651

Liu, Z. Bin, He, Y. L., Qu, Z. G., & Tao, W. Q. (2015). Experimental study of heat transfer and pressure drop of supercritical CO2 cooled in metal foam tubes. *International Journal of Heat and Mass Transfer*, *85*, 679–693. https://doi.org/10.1016/j.ijheatmasstransfer.2015.02.013

Lu, W., Zhang, T., & Yang, M. (2016). Analytical solution of forced convective heat transfer in parallel-plate channel partially filled with metallic foams. *International Journal of Heat and Mass Transfer*, *100*, 718–727. https://doi.org/10.1016/j.ijheatmasstransfer.2016.04.047

Mancin, S., Zilio, C., Rossetto, L., & Cavallini, A. (2010). *Experimental and analytical study of heat transfer and fluid flow through Aluminum foams.* AIP Conference Proceedings, American Institute of Physics. https://doi.org/10.1063/1.3453829

Mostafavi, M., & Meghdadi Isfahani, A. H. (2017). A new formulation for prediction of permeability of nano porous structures using lattice botzmann method. *Journal of Applied Fluid Mechanics*, *10*(2),

639–649. https://doi.org/10.18869/acadpub.jafm.73.239.26702

Muley, A., Kiser, C., Sundén, B., & Shah, R. K. (2012). Foam heat exchangers: A technology assessment. *Heat Transfer Engineering*, *33*(1), 42–51. https://doi.org/10.1080/01457632.2011.584817

Narasimmanaidu, S. R., Anuar, F. S., Sa'at, F. A. M., & Tokit, E. M. (2021). Numerical and experimental study of flow behaviours in porous structure of aluminium metal foam. *Evergreen Joint Journal of Novel Carbon Resource Sciences & Green Asia Strategy*, *8*(3), 658-666. https://doi.org/10.5109/4491842

Nield, D. A., & Bejan, A. (2005). *Convection in porous media*. 3rd ed., Berlin, Germany: Springer.

Nithyanandam, K., & Singh, P. (2022). Enhanced forced convection through thin metal foams placed in rectangular ducts. *Heat Transfer Engineering*, 837-852, https://doi.org/10.1080/01457632.2022.2102960

Odabaee, M., & Hooman, K. (2011). Application of metal foams in air-cooled condensers for geothermal power plants: An optimization study. *International Communications in Heat and Mass Transfer*, *38*(7), 838–843. https://doi.org/10.1016/j.icheatmasstransfer.2011.03.028

Odabaee, M., & Hooman, K. (2012). Metal foam heat exchangers for heat transfer augmentation from a tube bank. *Applied Thermal Engineering*, *36*(1), 456–463. https://doi.org/10.1016/j.applthermaleng.2011.10.063

Sener, M., Yataganbaba, A., & Kurtbas, I. (2016). Forchheimer forced convection in a rectangular channel partially filled with aluminum foam. *Experimental Thermal and Fluid Science*, *75*, 162–172. https://doi.org/10.1016/j.expthermflusci.2016.02.003

Shuja, S. Z., & Yilbas, B. S. (2007). Flow over rectangular porous block in a fixed width channel: Influence of porosity and aspect ratio. *International Journal of Computational Fluid Dynamics*, *21*(7–8), 297–305. https://doi.org/10.1080/10618560701624518

Sung, H. J., Kim, S. Y., & Hyun, J. M. (1995). Forced convection from an isolated heat source in a channel with porous medium. *International Journal of Heat and Fluid Flow*, *16*(6), 527–535. https://doi.org/10.1016/0142-727X(95)00032-L

T'Joen, C., De Jaeger, P., Huisseune, H., Van Herzeele, S., Vorst, N., & De Paepe, M. (2010). Thermo-hydraulic study of a single row heat exchanger consisting of metal foam covered round tubes. *International Journal of Heat and Mass Transfer*, *53*(15–16), 3262–3274. https://doi.org/10.1016/j.ijheatmasstransfer.2010.02.055

Tikadar, A., & Kumar, S. (2022). Investigation of thermal-hydraulic performance of metal-foam heat sink using machine learning approach. *International Journal of Heat and Mass Transfer*, *199*, 123438. https://doi.org/10.1016/j.ijheatmasstransfer.2022.123438

Trilok, G., Gnanasekaran, N., & Mobedi, M. (2021). Various trade-off scenarios in thermo-hydrodynamic performance of metal foams due to variations in their thickness and structural conditions. *Energies*, *14*(24). https://doi.org/10.3390/en14248343

Wang, H., Ying, Q. F., Lichtfouse, E., & Huang, C. G. (2023). boiling heat transfer in copper foam bilayers in positive and inverse gradients of pore density. *Journal of Applied Fluid Mechanics*, *16*(5), 973–982. https://doi.org/10.47176/jafm.16.05.1624

Xu, H. J., Qu, Z. G., Lu, T. J., He, Y. L., & Tao, W. Q. (2011). Thermal modeling of forced convection in a parallel-plate channel partially filled with metallic foams. *Journal of Heat Transfer*, *133*(9). https://doi.org/10.1115/1.4004209